

ORIGINAL RESEARCH

Open Access



Reactive power optimization of a distribution network with high-penetration of wind and solar renewable energy and electric vehicles

Biao Xu¹, Guiyuan Zhang¹ , Ke Li^{1*}, Bing Li¹, Hongyuan Chi², Yao Yao¹ and Zhun Fan¹

Abstract

As high amounts of new energy and electric vehicle (EV) charging stations are connected to the distribution network, the voltage deviations are likely to occur, which will further affect the power quality. It is challenging to manage high quality voltage control of a distribution network only relying on the traditional reactive power control mode. If the reactive power regulation potentials of new energy and EVs can be tapped, it will greatly reduce the reactive power optimization pressure on the network. Keeping this in mind, our research first adds EVs to the traditional distribution network model with new forms of energy, and then a multi-objective optimization model, with achieving the lowest line loss, voltage deviation, and the highest static voltage stability margin as its objectives, is constructed. Meanwhile, the corresponding model parameters are set under different climate and equipment conditions. Ultimately, the optimization model under specific scenarios is obtained. Furthermore, considering the supply and demand relationship of the network, an improved technique for order preference by similarity to an ideal solution decision method is proposed, which aims to judge the adaptability of different algorithms to the optimized model, so as to select a most suitable algorithm for the problem. Finally, a comparison is made between the constructed model and a model without new energy. The results reveal that the constructed model can provide a high quality reactive power regulation strategy.

Keywords Renewable energy, Electric vehicle, Multi-objective optimization, Pareto front, Reactive power optimization

1 Introduction

Renewable energy has characteristics of sustainability, cleanliness and, often, inexhaustible supply. Research has shown that renewable/new energy systems can not only meet active load demand of the power grid, but also achieve rapid reactive power regulation using power electronic devices connected to the network [1–3].

However, with large-scale renewable energy connecting to the distribution network, the existence of many power electronic devices in the power network can cause severe reactive power impact, which can seriously affect power quality and power system voltage stability [4]. In addition, because of the influence and unpredictability of the natural environment, there will be a great uncertainty in the reactive power regulation of the distribution network for new energy.

To achieve carbon neutrality, the demand for electric vehicles (EVs) increases in association with the need for emission reduction. EVs may participate in regulating the output of the power grid and trading energy with

*Correspondence:

Ke Li
ericlee@stu.edu.cn

¹ Shantou University, Shantou, China

² The AI Application and Innovation Center of China Mobile Communications Group Guangdong Co., Ltd., Shantou, China



© The Author(s) 2022, corrected publication 2023. **Open Access** This article is licensed under a Creative Commons Attribution 4.0 International License, which permits use, sharing, adaptation, distribution and reproduction in any medium or format, as long as you give appropriate credit to the original author(s) and the source, provide a link to the Creative Commons licence, and indicate if changes were made. The images or other third party material in this article are included in the article's Creative Commons licence, unless indicated otherwise in a credit line to the material. If material is not included in the article's Creative Commons licence and your intended use is not permitted by statutory regulation or exceeds the permitted use, you will need to obtain permission directly from the copyright holder. To view a copy of this licence, visit <http://creativecommons.org/licenses/by/4.0/>.

the grid based on vehicle to grid (V2G), to help realize benign interaction between EVs and the power grid. The bi-directional charging technology of EVs has great flexibility. A certain number of EVs connected to the distribution network can not only solve the problem of power storage, but also make a positive impact on the reactive power regulation of the distribution network. Therefore, to accelerate the transformation of energy structure and improve the overall reactive power regulation ability of the network, EVs may be used to optimize the reactive power regulation [5].

Reactive power optimization is a complex multi-objective optimization problem (MOP) with nonlinear, non-convex and discrete optimization variables [6] considering EVs and new energy types. In general, the traditional interior point or Newton method would be employed to optimize such kind of reactive power regulation model. The idea of these methods is to transform the MOP into a single objective optimization problem with a series of linear weights. However, it is impossible to give a relatively optimal control scheme for an MOP [7–10]. In contrast, it is more convenient to solve a complex multi-objective reactive power optimization problem with a multi-objective evolutionary algorithm (MOEA) based on Pareto front (PF). Also, the results of an MOEA are easier to understand.

Research in different fields has different approaches to reactive power optimization, and there is a variety of studies, especially in modeling. In [11], a three-stage relaxation-weightsum-correction based probabilistic reactive power optimization model is proposed, while [12] employs a mixed integer convex programming model in reactive power optimization. Both are utilized to address the uncertainties of wind power output. The pioneering work in [13] explores a cold-start linear branch flow model named modified DistFlow to obtain results with better accuracy, whereas [14] presents a novel comprehensive planning framework and optimizes from the perspective of technical, economic, and environmental benefits by considering distributed generation (DG) and EVs.

These different approaches have led to different methods being applied in reactive power optimization. In [15], a fully distributed reactive power optimization algorithm is shown to obtain the global optimum solution of non-convex problems easily, while [16] employs a decentralized voltage regulation method aimed at mitigating real-time nodal voltage variations. An improved particle swarm optimization algorithm is presented to minimize the sum of power consumption and investment cost of new reactive power compensation equipment in [17]. In [18], a multi-objective dimension-based firefly algorithm is applied to optimize power losses, emission and

cost in power systems. An efficient optimization method named hybrid multi-objective moth-flame optimization is proposed to solve the established MOP in [19]. To seek the optimal solutions for minimizing voltage deviation and network power losses, a meta-heuristic algorithm is proposed in [20]. However, there is still a lack of optimization on reactive power regulation when EVs are connected to distribution network.

This paper presents a reactive power optimization model where there is high penetration of wind, photovoltaic (PV) and EVs. Because of the rapid increase of the utilization rate of new energy and EVs, their impacts on reactive power optimization in a distribution network have reached a level that cannot be ignored. Most researchers are focused on single factor affecting the distribution network rather than multiple factors. This focus may lead to results not representing reality.

Therefore, in this paper, the recent Dual-Population-Based Evolutionary Algorithm for Constrained Multi-objective Algorithm (c-DPEA) is applied to tackle the established constrained MOP [21] and compared to other excellent MOEAs. First, on the basis of reactive power optimization considering a single objective, we present a compromise solution with MOEAs on MOPs. Then, an improved decision-making method, namely an improved technique for order preference by similarity to an ideal solution (TOPSIS), is proposed. It adjusts the importance of each objective according to the environmental impact in practical application. As a result, different objectives can be set with different importance weights to get more realistic solutions.

The rest of this paper is organized as follows. In Sect. 2, an advanced EV model is added to the traditional distribution network with new energy, while Sect. 3 introduces the optimization principle of c-DPEA and other algorithms, and presents the specific reactive power optimization application design process. The various standard node systems are used to simulate and test the distribution network connected with new energy and EVs in Sect. 4. Finally, Sect. 5 summarizes the work.

2 Mathematical model of reactive power optimization

2.1 Reactive power regulation model of wind power

The wind turbine model based on a doubly-fed induction generator (DFIG) is modified from [22], and shown in Fig. 1. DFIG converts the mechanical power captured by the wind turbine into electrical power. Meanwhile, it is fed into the grid by the DFIG stator and rotor through a back-to-back converter system, which is comprised of a rotor side converter and a grid side converter. According to the Betz equation, the input mechanical power P_m is directly related to the wind speed, as:

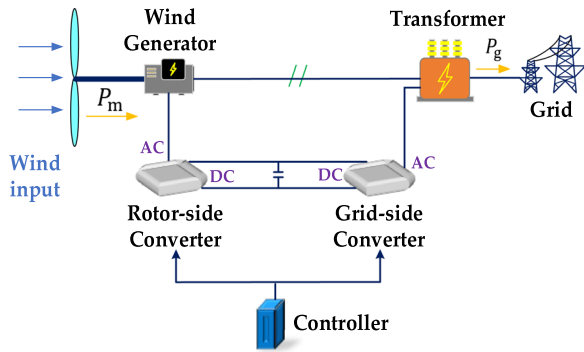


Fig. 1 Power generation model of DFIG

$$P_m = \frac{1}{2} C_p \rho \pi R^2 V^3 \tag{1}$$

where ρ is the air density, R means the radius of the wind turbine, V refers to the wind speed, C_p is a value related to blade tip speed ratio, λ , and pitch angle, β . λ can be expressed as:

$$\lambda = \frac{\omega_m \times R}{V} \tag{2}$$

where ω_m represents the rotation speed of the wind turbine.

In the ideal case, the active power can be considered as the maximum power point for tracking control (MPPT) [23], which is provided as follows.

$$P_g = \begin{cases} 0, & v_w < v_w^{in} \text{ or } v_w > v_w^{out} \\ P_w^{base} \frac{v_w - v_w^{in}}{v_w^{base} - v_w^{in}}, & v_w^{in} \leq v_w < v_w^{base} \\ P_w^{base}, & v_w^{base} \leq v_w \leq v_w^{out} \end{cases} \tag{3}$$

where P_w^{base} and v_w^{base} are the rated output and wind speed of the wind turbine, respectively.

However, the total reactive power fed into the grid is only related to the stator and the grid side converter rather than the rotor [24]. Thus, the total reactive power is given by:

$$\begin{cases} Q_{g,max} = Q_{s,max} + Q_{c,max} \\ Q_{g,min} = Q_{s,min} + Q_{c,min} \end{cases} \tag{4}$$

where $Q_{g,max}$ and $Q_{g,min}$ mean the upper and lower bounds of the reactive power injected into the power grid, respectively. Similarly $Q_{s,max}$ and $Q_{s,min}$ refer to the upper and lower bounds of the reactive power regulation range of the wind turbine stator side, while $Q_{c,max}$ and $Q_{c,min}$ are the upper and lower bounds of the reactive power regulation range of the grid side converter.

DFIG capacity limits are obtained by considering the stator and rotor maximum allowable currents, referred to as

the rated stator and rotor currents in steady state, whereas the generator total capacity limits are obtained by adding rotor power to the stator power. Thus, the reactive power regulation range of the stator side is affected by the maximum current constraints of the stator and rotor sides, as shown in (5)–(7).

$$\begin{cases} Q_{s,max} = \min \{ Q_{s1,max}, Q_{s2,max} \} \\ Q_{s,min} = \max \{ Q_{s1,min}, Q_{s2,min} \} \end{cases} \tag{5}$$

$$\begin{cases} Q_{s1,max} = -\frac{3U_s^2}{2\omega_1 L_s} + \sqrt{\left(\frac{3L_m}{2L_s} U_s I_{r,max}\right)^2 - \left(\frac{P_m}{1-s}\right)^2} \\ Q_{s1,min} = -\frac{3U_s^2}{2\omega_1 L_s} - \sqrt{\left(\frac{3L_m}{2L_s} U_s I_{r,max}\right)^2 - \left(\frac{P_m}{1-s}\right)^2} \end{cases} \tag{6}$$

$$\begin{cases} Q_{s2,max} = \sqrt{(U_s I_{s,max})^2 - \left(\frac{P_m}{1-s}\right)^2} \\ Q_{s2,min} = -\sqrt{(U_s I_{s,max})^2 - \left(\frac{P_m}{1-s}\right)^2} \end{cases} \tag{7}$$

where $Q_{s1,max}$ and $Q_{s1,min}$ refer to the upper and lower bounds of the reactive power regulation range of the wind turbine stator side under the maximum current constraint of the rotor side. $Q_{s2,max}$ and $Q_{s2,min}$ are the upper and lower bounds of the reactive power regulation range of the wind turbine stator side under the maximum current constraint of the stator side. L_s and L_m mean the stator inductance and excitation inductance, respectively. $I_{r,max}$ and $I_{s,max}$ are the maximum current values of the rotor side and stator side, s is the rotor slip, ω_1 is the angular velocity of synchronous rotation, and U_s is the stator voltage.

The reactive power of the grid side converter is limited by its capacity and the transmitted active power:

$$\begin{cases} Q_{c,max} = \sqrt{S_{c,max}^2 - \left(\frac{sP_m}{1-s}\right)^2} \\ Q_{c,min} = -\sqrt{S_{c,max}^2 - \left(\frac{sP_m}{1-s}\right)^2} \end{cases} \tag{8}$$

where $S_{c,max}$ is the capacity of the grid side converter.

2.2 Reactive power regulation model of PV

The flow of PV generation is shown in Fig. 2. Small-scale PV is related to some environmental factors, such as the current solar irradiation and temperature [25]. The active power output P_{pv} is considered as MPPT in the ideal state. Thus, P_{pv} can be presented as:

$$P_{pv} = P_{pv}^{base} [1 + \alpha_{pv} \cdot (T - T_{ref})] \cdot \frac{S_{pv}}{1000} \tag{9}$$

where P_{pv}^{base} refers to the rated total power of PV connected to the distribution network, α_{pv} is the temperature

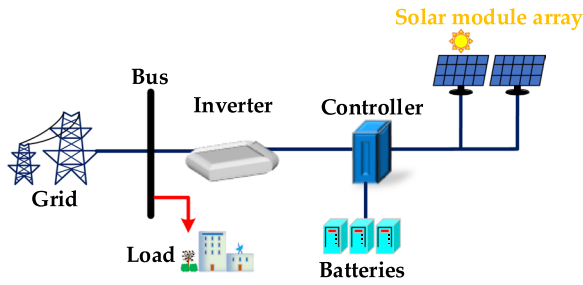


Fig. 2 Schematic diagram of PV generation

conversion coefficient of PV, T is the temperature at the current recording time, T_{ref} means a set reference temperature value, and s_{pv} is the solar irradiation at the current time.

The electric energy generated by PV is usually direct current (DC), and it is thus necessary to use a PV inverter to convert it into alternating current (AC) with the same frequency as the distribution network. Therefore, the influence of inverter capacity and active power output should be considered when calculating the regulation range of PV reactive power output, shown as:

$$\begin{cases} Q_{pv,max} = \sqrt{(S_{pv})^2 - (P_{pv})^2} \\ Q_{pv,min} = -\sqrt{(S_{pv})^2 - (P_{pv})^2} \end{cases} \quad (10)$$

where $Q_{pv,max}$ and $Q_{pv,min}$ refer to the upper and lower bounds of reactive power regulation range of the PV equipment. S_{pv} is the capacity of the PV inverter.

2.3 Reactive power regulation model of EVs

EVS can be regarded as small energy storage equipment. In addition, the converters of EV charging piles have good flexibility in regulating active and reactive power. Therefore, the addition of EVs can adapt to the development of reactive power optimization in a distribution network. While establishing a two-way charging relationship with the distribution network, EVs can provide significant reactive power regulation. A simplified working principle of the EVs is shown in Fig. 3. The electric energy in the power grid is three-phase AC. Thus, there are converter circuits in the EV charging piles to convert AC into DC, and then provide DC electric energy to the high-frequency DC-DC power converters. The battery energy management system will further optimize the DC input to the battery. When the EVs are connected to the charging piles, they can act as generators in the distribution network if the remaining energies exceed a certain threshold. Otherwise, the distribution network will transmit energies to charge the EVs [26]. The relationship between active power and converter parameters can be obtained as follows:

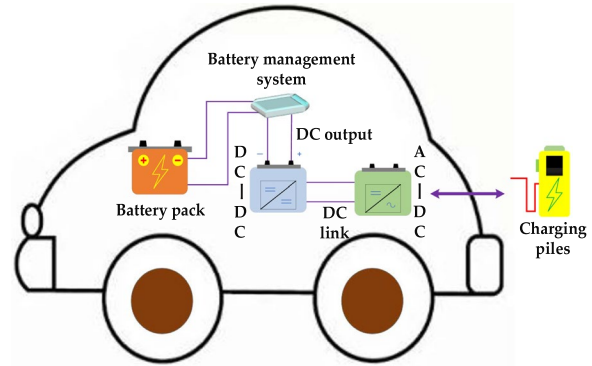


Fig. 3 Schematic diagram of bi-directional charger for EVs

$$P_{car} = \frac{V_s V_c \sin(\delta)}{\omega L_c} \quad (11)$$

where P_{car} is the input or output active power of the EV, and V_s and V_c are the grid and charging piles voltages. δ is the phase difference between V_s and V_c , ω is the angular frequency of the AC system, and L_c is the total interface inductance, including the line inductance and the charger filter inductance between the charger and the grid.

The reactive power regulation range of EVs is similar to PV, shown as:

$$\begin{cases} Q_{car,max} = \sqrt{(S_{car})^2 - (P_{car})^2} \\ Q_{car,min} = -\sqrt{(S_{car})^2 - (P_{car})^2} \end{cases} \quad (12)$$

where $Q_{car,max}$ and $Q_{car,min}$ represent the upper and lower bounds of reactive power regulation range of EVs. S_{car} is the capacity of the converters in the charging piles.

2.4 Objective function

There are three objectives to be optimized in this research. Line loss minimization belongs to the economic index of the power grid, while voltage deviation [27] minimization and static voltage stability margin maximization [28] are the indices affecting power grid performance and security. However, there is a hidden contradiction between the objectives. In order to obtain a PF with excellent convergence and diversity, an MOEA is used to handle the three objectives, and a Pareto optimal set is selected under certain circumstances. Particularly, in order to minimize the three objectives simultaneously, it is necessary to convert the maximized static voltage stability margin first. One of the methods is to convert it into solving the reciprocal of the minimum singular value of the minimum convergent power flow Jacobian matrix. In short, the minimization of function f_3 is equivalent to the maximization of the static voltage stability margin. The equations of the three objective functions are presented as follows.

$$\begin{cases} \min f_1 = \sum_{i,j \in N_L} g_{ij} (V_i^2 + V_j^2 - 2V_i V_j \cos \theta_{ij}) \\ \min f_2 = \sum_{j \in N_i} (V_j - V_j^*)^2 \\ \min f_3 = 1/\delta_{\min} \end{cases} \quad (13)$$

where f_1 , f_2 and f_3 mean the power losses, voltage deviation and singular value reciprocal of the Jacobian matrix of the system, respectively. V_i and V_j refer to the voltage amplitudes of the i th and j th nodes. θ_{ij} is the phase angle difference between the i th and j th nodes, g_{ij} presents the admittance between the i th and j th nodes, N_i and N_L mean the total node set and all branch set, V_j^* is the rated voltage of the j th node, and δ_{\min} represents the minimum singular value of the system Jacobian matrix.

2.5 Constraint condition

IN the process of reactive power optimization, the scope of each parameter and condition should be taken into consideration [29].

(1) Power flow equality constraints:

$$\begin{cases} P_{Gi} - P_{Di} - V_i \sum_{j \in N_i} V_j (g_{ij} \cos \theta_{ij} + b_{ij} \sin \theta_{ij}) = 0, i \in N_0 \\ Q_{Gi} - Q_{Di} - V_i \sum_{j \in N_i} V_j (g_{ij} \sin \theta_{ij} - b_{ij} \cos \theta_{ij}) = 0, i \in N_{PQ} \end{cases} \quad (14)$$

where P_{Gi} and Q_{Gi} represent the active power and reactive power of the i th generation node, respectively. P_{Di} and Q_{Di} are the active power and reactive power demand of the i th node. b_{ij} refers to the susceptance between the i th and j th nodes, N_0 presents the node set except the balance node, and N_{PQ} is the PQ node set.

(2) Generator constraints:

$$\begin{cases} Q_{Gi}^{\min} \leq Q_{Gi} \leq Q_{Gi}^{\max}, i \in N_G \\ V_{Gi}^{\min} \leq V_{Gi} \leq V_{Gi}^{\max}, i \in N_G \end{cases} \quad (15)$$

where Q_{Gi}^{\min} and Q_{Gi}^{\max} are the lower and upper limits of reactive power regulation of the i th generator. Q_{Gi} refers to the reactive power currently injected into the grid by the i th generator and V_{Gi}^{\min} and V_{Gi}^{\max} are the lower and upper limits of output voltage of the i th generator. V_{Gi} is the current output voltage of the i th generator, and N_G is the generator set.

(3) Generation ramp constraint (GRC): In addition to meeting the constraints of reactive power output and voltage, the generation units also need to meet

certain constraints on regulation active power output [30, 31].

$$-\Delta P_j^{\text{rate}} \leq \frac{\Delta P_j^{\text{out}}(c) - \Delta P_j^{\text{out}}(c-1)}{\Delta T} \leq \Delta P_j^{\text{rate}} \quad (16)$$

where ΔP_j^{rate} means the maximum ramp rate of the j th generation unit, $\Delta P_j^{\text{out}}(c)$ denotes the regulation power output of the j th generation unit at the c th control interval, and ΔT refers to the time cycle of generation units dispatch.

(4) Start-stop constraint:

$$\sum_{j \in O} \max \{ \Delta P_j^{\text{out}}(c) - R_j(c), \Delta P_j^{\text{min}}(c) \} > P_D(c+1) \quad (17)$$

where O means the set of operating generation units at the c th control interval, and $R_j(c)$ is the downward ramp rate of the j th generation unit. $\Delta P_j^{\text{min}}(c)$ represents the minimum active output of the j th generation unit in the c th control interval, and $P_D(c+1)$ means the total active power demand of the power grid at the $(c+1)$ th interval.

(5) Reactive power compensation device and transformer tap constraint:

$$\begin{cases} Q_{Ci}^{\min} \leq Q_{Ci} \leq Q_{Ci}^{\max}, i \in N_C \\ T_h^{\min} \leq T_h \leq T_h^{\max}, h \in N_T \end{cases} \quad (18)$$

where Q_{Ci}^{\min} and Q_{Ci}^{\max} refer to the lower and upper limits of the capacity of the i th reactive power compensation device. T_h^{\min} and T_h^{\max} mean the lower and upper limits of the regulation range of the h th transformer tap. N_C is the set of reactive power compensation devices, and N_T denotes the set of transformer taps.

(6) Security Constraint:

$$\begin{cases} V_i^{\min} \leq V_i \leq V_i^{\max}, i \in N_{PQ} \\ |S_l| \leq S_l^{\max}, l \in N_L \end{cases} \quad (19)$$

where V_i^{\min} and V_i^{\max} are the lower and upper voltage limits of the i th node. S_l is the apparent power of the l th line and S_l^{\max} is the transmission power limit of the l th line.

3 Optimization framework and algorithm comparison

3.1 Brief description of the optimization process of c-DPEA, CCMO and WOF

In general, constrained multi-objective optimization problems (CMOP) are more challenging than unconstrained MOPs [32–35]. In the constrained environment, some search spaces will be directly excluded by the constraint factors, and the algorithm can only search for optimization over a narrow feasible region, or even make all search spaces infeasible in extreme cases, resulting in a final failure to get the optimization results [21, 36].

In order to address this kind of CMOP, c-DPEA is applied for reactive power optimization. The main innovation of this algorithm is that two populations are used to co-evolve for the problem. They deal with the infeasible solutions in different ways. Population 1 can find better points in infeasible regions more conveniently and quickly, while the optimization process of population 2 can approach the front faster. This kind of co-evolution obtains a win–win result, as it emphasizes convergence and diversity in two different populations.

A co-evolutionary constrained multi-objective optimization framework (CCMO) also proposes the idea of two populations [37]. This framework evolves one population to solve the original CMOP and evolves another to solve a helper problem derived from the original. It is worth noting that the two populations will share their useful information by their own optimizer separately.

A weighted optimization framework (WOF) is employed to deal with this problem here [38]. A WOF can be seen as a generic method that can be used with any population-based meta-heuristic algorithm. This algorithm is intended to solve multi-objective optimization problems with a large number of decision variables.

3.2 Application design of algorithms in reactive power optimization of a distribution network

(1) How to handle variables, especially the discrete ones:

Reactive power optimization includes continuous variables and discrete variables. These need to be discussed separately in iteration. Continuous variables can be iterated according to normal optimization, while discrete variables need to be rounded by continuous spatial values. In addition, for the values of the discrete variables, the upper and lower bounds of the continuous spaces correspond to the upper and lower bounds of discrete variables. For example, the decision variables are set to 17 in the 33-bus system, including several new energy outputs, charging and battery change stations, reactive

power compensation devices and a group of transformer taps. Then, the upper and lower bounds of reactive power can be calculated from Sect. 2.

(2) How to evaluate the fitness function:

It is necessary to consider the objectives and constraints in reactive power optimization in an actual distribution network. In the process of optimization iteration, the individuals must satisfy the condition provided in (13) to calculate the power flow. Consequently, the fitness function can be designed as:

$$f_{fit,t}(x^i) = f_t(x^i) + \eta q, \quad t \in T \tag{20}$$

where T is the set of objective functions, and t represents the t th objective value in the set of objective functions. $f_t(x^i)$ and $f_{fit,t}(x^i)$ are the values of the objective and fitness functions, respectively. η is a penalty coefficient which is often set as a larger constant, and q is the number of objectives that do not meet the constraints.

For example, the reactive power optimization flow chart of c-DPEA for the model is shown in Fig. 4. The power flow to obtain the solution set of the objective function value needs to be calculated first. Then the method of adjusting the fitness function (18) is employed. Finally, the algorithm enters the next iteration.

3.3 Application for improved TOPSIS in comparing optimization results of different algorithm

In some real situations, the importance of different objectives will change with different factors. Similarly, different algorithms may have different optimization results because of the change of real parameters. We propose an improved adaptive Technique for Order Preference by Similarity to an Ideal Solution (TOPSIS) decision method to compare the optimization results of the different algorithms in different cases.

Line loss and voltage deviation can be the minimum index in the decision method. However, the static voltage stability margin should be the maximum index. The maximum index needs to be transformed into the minimum index by the method of finding the reciprocal. If there are n objects to be evaluated and m indices to be evaluated, an evaluation matrix can be obtained, as:

$$Z = \begin{bmatrix} z_{11} & \cdots & z_{1m} \\ \vdots & \ddots & \vdots \\ z_{n1} & \cdots & z_{nm} \end{bmatrix} \tag{21}$$

The general calculation of the decision method is as follows:

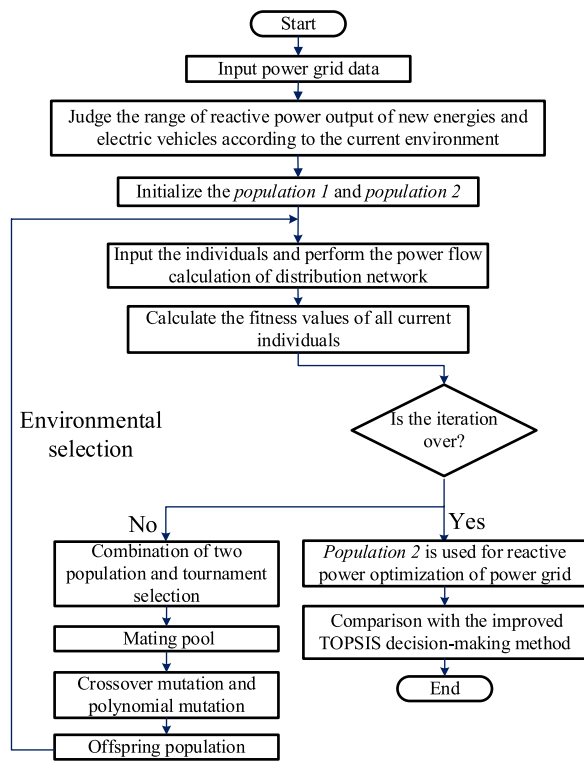


Fig. 4 Flow chart of c-DPEA for reactive power optimization

For the objective function of the three very small indicators mentioned above, the value of the objective function needs to be transformed into the maximum index. Then, TOPSIS can be employed to judge the advantages and disadvantages of the different algorithms. It is worth noting that the result range of S_i must satisfy the condition of $0 < S_i < 1$. The larger S_i is, the closer it is to the objective maximum. A threshold will be set in this process. When the S_i obtained from TOPSIS is greater than the threshold and less than 1 after the optimization, the scores of this specific algorithm will be increased by 1. The higher the score is, the higher the matching degree between the algorithm and the optimization model is.

The weights of line loss, voltage deviation and static voltage stability margin are set as w_1 , w_2 and w_3 , respectively. There is a PV coefficient k_1 , which changes with the increase or decrease of solar irradiation or temperature difference. Similarly, the wind power coefficient k_2 varies according to the wind speed. k_1 and k_2 affect the weight w_2 of voltage deviation by a feedback link. At the same time, a line loss threshold will be set. If the optimization result is less than this threshold, the line loss weight will be increased according to a certain proportion. Finally, two or three objective weights are imported to calculate the fitness score of the algorithm.

$$Z^+ = (\max\{z_{11}, z_{21}, \dots, z_{n1}\}, \max\{z_{12}, z_{22}, \dots, z_{n2}\}, \dots, \max\{z_{1m}, z_{2m}, \dots, z_{nm}\}) \quad (22)$$

$$Z^- = (\min\{z_{11}, z_{21}, \dots, z_{n1}\}, \min\{z_{12}, z_{22}, \dots, z_{n2}\}, \dots, \min\{z_{1m}, z_{2m}, \dots, z_{nm}\}) \quad (23)$$

$$D_i^+ = \sqrt{\sum_{j=1}^m (Z_j^+ - z_{ij})^2}, \quad i = 1, 2, \dots, n \quad (24)$$

$$D_i^- = \sqrt{\sum_{j=1}^m (Z_j^- - z_{ij})^2}, \quad i = 1, 2, \dots, n \quad (25)$$

$$S_i = \frac{D_i^-}{D_i^+ + D_i^-} \quad (26)$$

where Z^+ means the maximum value and Z^- is the minimum value. D_i^+ refer to the distance between the i th evaluation object and the maximum value, while D_i^- is the distance between the i th evaluation object and the minimum value. S_i is the non-normalized score of the i th evaluation object.

4 Example analysis

4.1 Simulation model

The topology of the 33-bus system is shown in Fig. 5. In this work, the installed capacities of DFIG and PV are set as 300 kW and 21 kW, respectively, while the total capacity of EV charging and battery change station is 80 kW. The active power output of the wind turbine affected by wind speed can be divided into three stages, with v_w^{in} , v_w^{out} and v_w^{base} set as 3 m/s, 25 m/s and 12 m/s, respectively. The initial solar irradiation is 600 W m^{-2} in the PV system, the temperature conversion coefficient is 0.2 and the temperature difference can be regarded as a fixed value of $2 \text{ }^\circ\text{C}$. New types of energy are affected by different environmental factors, so the initial parameter differences are explained in Tables 1 and 2.

EV is a great uncontrollable factor, and can be regarded as an uncertain load or a small battery. Here we have 3 and 6 EV charging and battery change stations in the 33-bus system and 118-bus system, respectively. However, the number of EVs in each station is set to 10 and the power of a single EV is 0–10 kW, so the total power of EVs at each station will always be within the range of 0–100 kW. Then, the state of EV batteries will be determined by its own state of charge (SOC). The EVs are in charging state within the SOC of

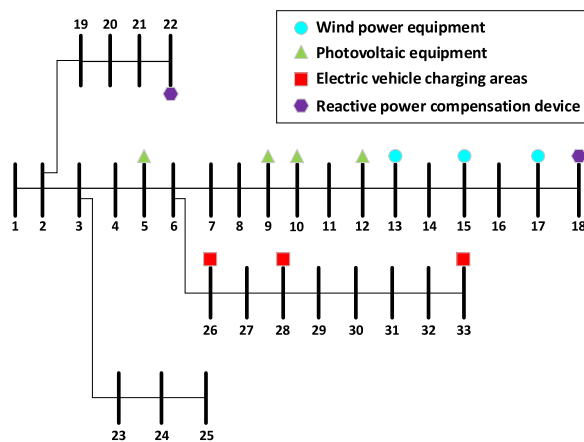


Fig. 5 Topologies of the IEEE 33-bus system

Table 1 Parameters of wind and PV generators and EVs in the IEEE 33-bus distribution system

Number	Wind speed (m s ⁻¹)	Solar irradiation (W m ⁻²)	Active power (kW)	Reactive capacity (kVar)
<i>PV equipment</i>				
1		600	12.00	[-17.23,17.23]
2		700	14.00	[-15.65,15.65]
3		800	16.00	[-13.60,13.60]
4		900	18.00	[-10.82,10.82]
<i>Wind power generation</i>				
1	9		200.00	[-136.60,151.11]
2	11		266.67	[-92.13,121.48]
3	13		300.00	[-69.90,106.67]
<i>EV charging and battery change station</i>				
1			-42.80	[-67.59,67.59]
2			-49.02	[-63.22,63.22]
3			-31.93	[-73.35,73.35]

0–60% while they are in transmission state within SOC of 60–100%.

The default population and iteration are 50 and 50, respectively, so the optimization results can be obtained quickly. However, it is necessary to increase the respective population and iteration to 200 and 50 in the three-objective optimization, so that comprehensive results can be obtained and the error can be reduced to some extent. In this work, the three algorithms are independently applied in the same software environment.

The optimization variables include reactive power compensation devices, transformer taps, new energy generators, EV charging and battery change stations, while the variations of wind speed and solar irradiation are only set

to several regular stages. More practical problems will be gradually realized in subsequent research.

4.2 Analysis of optimization results

The PF obtained by different algorithms for bi-objective and three-objective in the IEEE 33-bus system are shown in Figs. 6 and 7, respectively. It is seen from Fig. 6 that CCMO and c-DPEA can find better PF in the optimization process. By comparison, the optimization degree of WOF is lower than the other two. The PF of WOF is much narrower than those of CCMO and c-DPEA. WOF has the most dominated solutions in several simulation experiments. From Table 3, the HV and spacing also present the outstanding uniformity of c-DPEA and poor uniformity of WOF. For CCMO, it has the characteristic of being mediocre. Its HV and spacing are inferior to c-DPEA although it can obtain good PF. In the three-objective optimization in Fig. 7, the optimized Pareto surface (PS) of CCMO is concentrated in a small area in the middle while WOF has the advantage of uniform distribution. By contrast, c-DPEA shows the advantages of fast optimization speed, uniform PS and great optimization degree. From Table 4, the indices of c-DPEA cover almost all the optimal values for both the 33-bus and 118-bus systems. In this regard, c-DPEA gives satisfactory results with excellent equilibrium and stability. Its results are moderate while being optimized as much as possible.

Here, 0.7 is set as the threshold and the initial score of each algorithm is 0. Fifty individuals in the optimized population are randomly selected to calculate the fitness degree. If the fitness degree is greater than the threshold, the score is increased by 1. In order to reduce contingency and error, the optimization results of four different systems are added to calculate the fit. All data in the tables are average values. Tables 5 and 6 shows the fit scores of bi-objective and three-objective, respectively. In Table 5, c-DPEA shows the advantages in a small distribution network while WOF shows its advantages in the 118-bus system. Although CCMO has excellent scalability in PE, its score in practical model is not satisfactory. In Table 6, the average fit scores of c-DPEA are slightly higher than those of the other two algorithms. However, CCMO has the best performance in the 39-bus system. These data directly prove that c-DPEA is still more stable and suitable in different situations than the other two algorithms when the number of objectives is different.

In Tables 7 and 8, the work is divided into three different cases. The first case shows the influence of new energy and EVs while the last two consider only one of them. In longitudinal comparison, the indices of c-DPEA

Table 2 Parameters of wind and PV generators and EVs in the 118-bus distribution system

Number	Wind speed (m s ⁻¹)	Solar irradiation (W m ⁻²)	Active power (kW)	Reactive capacity (kVar)
<i>PV equipment</i>				
1		350	7.00	[- 21.91,21.91]
2		450	9.00	[- 21.17,21.17]
3		550	11.00	[- 20.20,20.20]
4		650	13.00	[- 18.97,18.97]
5		750	15.00	[- 17.44,17.44]
6		850	17.00	[- 15.49,15.49]
7		950	19.00	[- 12.96,12.96]
8		1050	21.00	[- 9.38,9.38]
<i>Wind power generation</i>				
1	9		200.00	[- 136.60,151.11]
2	11		266.67	[- 92.13,121.48]
3	13		300.00	[- 69.90,106.67]
4	15		300.00	[- 69.90,106.67]
5	17		300.00	[- 69.90,106.67]
6	19		300.00	[- 69.90,106.67]
<i>EV charging and battery change station</i>				
1			- 52.03	[- 60.77,60.77]
2			- 38.09	[- 70.35,70.35]
3			- 58.54	[- 54.52,54.52]
4			- 29.22	[- 74.47,74.47]
5			64.20	[- 47.74,47.74]
6			- 58.44	[- 54.64,54.64]

largely become the optimal solutions in the first case for both the 33-bus and 118-bus systems, as C-DPEA has better comprehensive capability and evenness. In other words, this algorithm can exert its excellent optimization ability in the face of these situations. From the

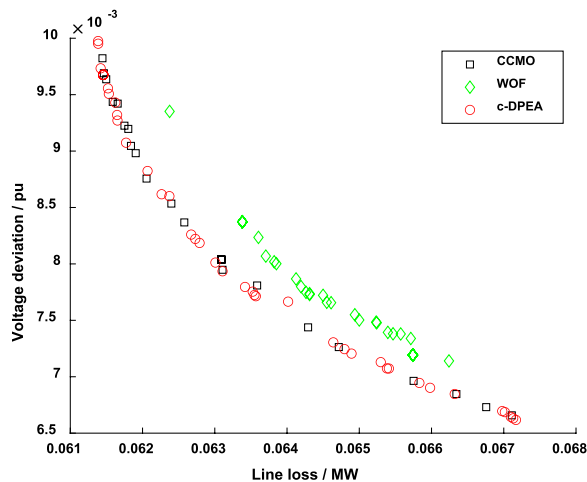


Fig. 6 PF comparison of the different algorithms for bi-objective in IEEE 33-bus system

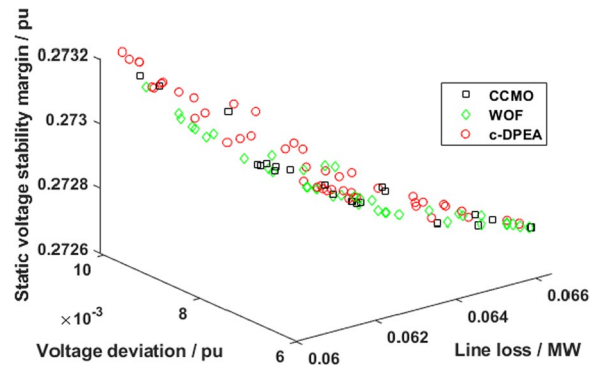


Fig. 7 PF comparison of the different algorithms for three-objective in the IEEE 33-bus system

Table 3 Indices comparison of the three algorithms for bi-objective in different systems

Index	System	c-DPEA	CCMO	WOF
HV	33-bus	0.0592	0.0565	0.0391
	118-bus	0.0092	0.0090	0.0095
Spacing	33-bus	1.1271e-04	2.0299e-04	2.8984e-04
	118-bus	2.3498e-04	2.0475e-04	2.7083e-04

The significance of bold means the optimal value among the datum in the same row

Table 4 Indices comparison of the three algorithms for three-objective in different systems

Index	System	c-DPEA	CCMO	WOF
HV	33-bus	0.0057	0.0054	0.0053
	118-bus	8.1802e-04	8.1715e-04	8.5152e-04
Spacing	33-bus	1.5148e-04	2.5288e-04	1.9351e-04
	118-bus	1.8061e-04	2.2140e-04	4.2970e-04

The significance of bold means the optimal value among the datum in the same row

Table 5 Average fit scores of bi-objective for different algorithms

System	c-DPEA	CCMO	WOF
14-bus	19.4	18.2	11.6
33-bus	19.0	17.6	16.0
39-bus	18.4	18.8	14.2
118-bus	20.2	19.8	23.4

The significance of bold means the optimal value among the datum in the same row

Table 6 Average fit scores of three-objective for different algorithms

System	c-DPEA	CCMO	WOF
14-bus	20.0	18.2	11.6
33-bus	11.6	11.0	9.0
39-bus	18.4	18.8	14.6
118-bus	19.8	19.0	13.8

The significance of bold means the optimal value among the datum in the same row

Table 7 Results of the IEEE 33-bus system in different circumstances

Algorithm	Indices	New energies and EVs and algorithms	New energies and algorithms	EVs and algorithms
c-DPEA	HV	0.0592	0.0352	0.0170
	Spacing	1.1271e-04	1.1571e-04	1.1312e-04
CCMO	HV	0.0565	0.0347	0.0170
	Spacing	2.0299e-04	2.0301e-04	1.4139e-04
WOF	HV	0.0391	0.2728	0.0141
	Spacing	2.1984e-04	2.2875e-04	1.7113e-04

The significance of bold means the optimal value among the datum in the same row

Table 8 Results of the IEEE 118-bus system in different circumstances

Algorithm	Indices	New energies and EVs and algorithms	New energies and algorithms	EVs and algorithms
c-DPEA	HV	8.1802e-04	8.1631e-04	8.1622e-04
	Spacing	1.8061e-04	1.9787e-04	1.8345e-04
CCMO	HV	8.1715e-04	8.1642e-04	8.0769e-04
	Spacing	1.7140e-04	1.9871e-04	1.6630e-04
WOF	HV	8.5152e-04	8.3113e-04	8.3282e-04
	Spacing	4.2970e-04	4.7741e-04	3.8431e-04

The significance of bold means the optimal value among the datum in the same row

perspective of horizontal comparison, the case with only EVs has good performance in spacing. This is because the addition of EVs may reduce the reactive power optimization pressure of a distribution network. Thus, some losses of the distribution network will be greatly reduced with new energy and EVs. This directly affects the economy and security of the distribution network in practice.

In Figs. 8 and 9, the effects of different wind speeds and solar irradiation in the optimization results are shown.

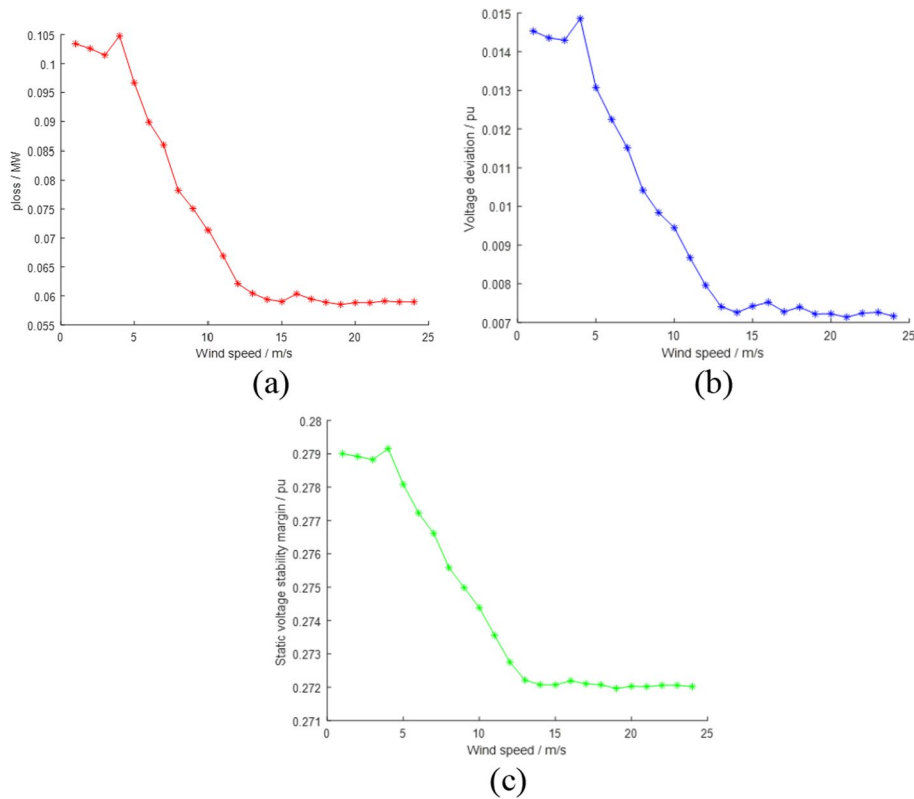


Fig. 8 Effects of different wind speed on c-DPEA optimization (three-objective) **a** Line loss; **b** Voltage deviation; **c** Static voltage stability margin

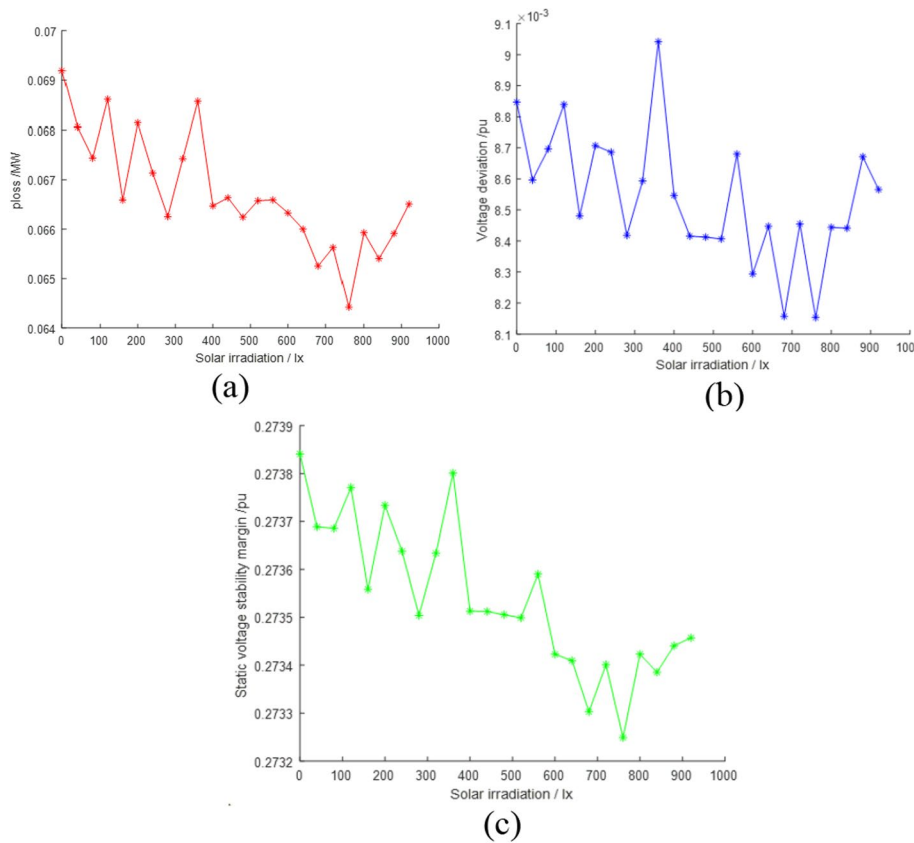


Fig. 9 Effects of different solar irradiation on c-DPEA optimization (three-objective) **a** Line loss; **b** Voltage deviation; **c** Static voltage stability margin

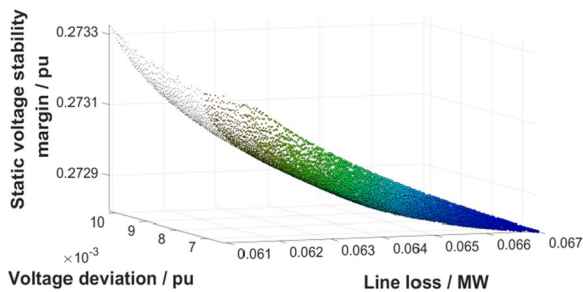


Fig. 10 Optimization results of reactive power compensation device not connected to distribution network by c-DPEA

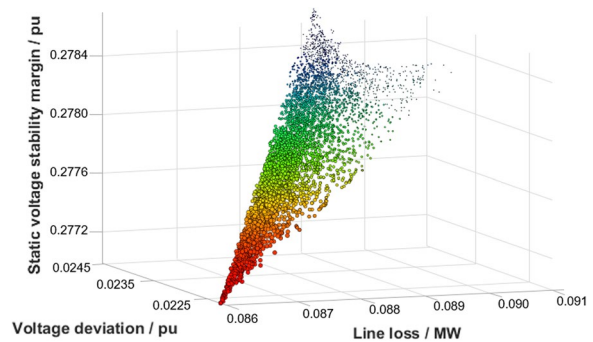


Fig. 11 Optimization results of reactive power compensation device connected to distribution network by c-DPEA

The simulation is carried out when other variables are consistent. In Fig. 8, the three objectives decrease significantly with the increase of wind speed, especially in the range of 5–13 m/s. The change trend of the three objectives is not obvious for the increase of solar irradiation in Fig. 9. However, the three objectives still have an overall downward trend. Their variations occur around the average values, but the deviation rates are not high. Thus, c-DPEA is fully applicable to this distribution network model. Although there are various influencing factors

such as climate in real life, this algorithm can get the results stably and quickly.

Figures 10 and 11 compare the results with and without the reactive power compensation devices in the distribution network. The initial conditions of the two situations are the same based on c-DPEA. In order to draw a more complete and clearer graph, 5000 individuals and 50 iterations are set in the two different situations. Figure 10 is obtained by ignoring the reactive power compensation

device, and its distribution approximates a smooth surface while the solutions are evenly distributed. For the optimization results with a reactive power compensation device shown in Fig. 11, the distribution change of the solution is small and is concentrated in a narrow long band compared with the former. The data show that the optimal values of line loss and voltage deviation after adding a reactive power compensation device are slightly higher than those without the device. In contrast, the optimal results of the latter are obviously better than the former in solving the maximum value of the static voltage stability margin. Consequently, c-DPEA can be used in general situations in the multi-objective optimization task of a real distribution network. It can obtain different optimization priority results in the face of optimization requirements in different situations.

5 Conclusion

To show the adaptability of MOEAs to a distribution network with new energy and EVs, this paper constructs a large framework, summarized as follows:

- (1) The distribution network model with new energy and EVs is built to reflect the reactive power regulation potential in various types of distribution network.
- (2) Several MOEAs are applied to the above model. Moreover, their operational process and applicability to specific models are described in detail. Comparing with different algorithms, both CCMO and WOF are slightly inferior to c-DPEA from different indices. c-DPEA has the characteristic of stable adaptation in optimization problems among different environments. The comprehensive capacity of c-DPEA and the evenness of its PF are shown in Sect. 4. However, its advantages in large systems are not as significant as those in small systems, especially in the 39-bus system. It also explains that there are a certain number of dominated solutions in PF for c-DPEA.
- (3) An adaptive strategy is added to the improved TOPSIS method with the precision of a distribution network model. The strategy can change the priority of an objective according to its actual needs during the optimization, with the more important objectives receiving more attention.
- (4) This research also attempts to examine and verify whether the proposed model is affected by various environmental factors, e.g., the change of wind speed and solar irradiation, or the addition and deletion of reactive power compensation devices. Taking c-DPEA as an example, it shows that the

model has a good ability to adapt to the actual changeable environment.

In summary, the rational use of the proposed method can provide an alternative idea for the multi-objective optimization of a distribution network in the future.

Acknowledgements

Not applicable.

Author contributions

B. Xu performed the sections of abstract and introduction. G. Y. Zhang obtained and analyzed the final experimental data. K. Li and B. Li proposed the integrated model of new energies and EVs. H. Y. Chi was a major contributor in the choice of algorithms and the improvement of TOPSIS method. Y. Yao provided suggestions on the construction and embellishment of flow chart. Z. Fan interpreted the data and integrated the conclusions.

Funding

This work was jointly supported by National Key R&D Program of China (2021ZD0111502), National Natural Science Foundation of China (51907112, U2066212), Natural Science Foundation of Guangdong Province of China (2019A1515011671, 2021A1515011709), Scientific Research Starting Foundation of Shantou University (NTF19028, NTF20009). The funding body have played a role in the purchase of experimental equipment and expert consultation.

Availability of data and materials

Not applicable.

Declarations

Competing interests

The authors declare that they have no known competing financial interests or personal relationships that could have appeared to influence the work reported in this paper.

Received: 8 July 2022 Accepted: 25 November 2022

Published: 13 December 2022

References

1. Molina-Garcia, A., Mastromauro, R. A., Garcia-Sanchez, T., Pugliese, S., Liserre, M., & Stasi, S. (2017). Reactive power flow control for PV inverters voltage support in LV distribution networks. *IEEE Transactions on Smart Grid*, *8*(1), 447–456.
2. Burke, M. J., & Stephens, J. C. (2018). Political power and renewable energy futures: A critical review. *Energy Research & Social Science*, *35*, 78–93.
3. Sequeira, T. N., & Santos, M. S. (2018). Renewable energy and politics: A systematic review and new evidence. *Journal of Cleaner Production*, *192*, 553–568.
4. Zheng, W. Y., & Wu, W. C. (2019). Distributed multi-area load flow for multi-microgrid systems. *IET Generation, Transmission & Distribution*, *13*(3), 327–336.
5. Mitra, P., & Venayagamoorthy, G. K. (2010). Wide area control for improving stability of a power system with plug-in electric vehicles. *IET Generation, Transmission & Distribution*, *4*(10), 1151–1163.
6. Mahmud, N., & Zahedi, A. (2016). Review of control strategies for voltage regulation of the smart distribution network with high penetration of renewable distributed generation. *Renewable and Sustainable Energy Reviews*, *64*, 582–595.
7. Mohseni-Bonab, S. M., Rabiee, A., & Mohammadi-Ivatloo, B. (2016). Voltage stability constrained multi-objective optimal reactive power dispatch under load and wind power uncertainties: A stochastic approach. *Renewable Energy*, *85*, 598–609.

8. Guo, Y. F., Gao, H. L., Wu, Q. W., Ostergaard, J., Yu, D. C., & Shahidehpour, M. (2019). Distributed coordinated active and reactive power control of wind farms based on model predictive control. *International Journal of Electrical Power & Energy Systems*, *104*, 78–88.
9. Wu, J. Y., Shi, C., Shao, M. Y., An, R., Zhu, X. W., Huang, X., & Cai, R. (2019). Reactive power optimization of a distribution system based on scene matching and deep belief network. *Energies*, *12*(17), 3246.
10. Sarkar, M. N. I., Meegahapola, L. G., & Datta, M. (2018). Reactive power management in renewable rich power grids: A review of grid-codes, renewable generators, support devices, control strategies and optimization algorithms. *IEEE Access*, *6*, 41458–41489.
11. Chen, S. H., Hu, W. H., Du, Y. F., Wang, S. X., Zhang, C. X., & Chen, Z. (2022). Three-stage relaxation-weightsum-correction based probabilistic reactive power optimization in the distribution network with multiple wind generators. *International Journal of Electrical Power & Energy Systems*, *141*, 108146.
12. Ding, T., Liu, S. Y., Yuan, W., Bie, Z. H., & Zeng, B. (2016). A two-stage robust reactive power optimization. *IEEE Transactions on Sustainable Energy*, *7*(1), 301–311.
13. Yang, T. S., Guo, Y., Deng, L. R., Sun, H. B., & Wu, W. C. (2021). A linear branch flow model for radial distribution networks and its application to reactive power optimization and network reconfiguration. *IEEE Transactions on Smart Grid*, *12*(3), 2027–2036.
14. Adetunji, K. E., Hofsajer, I. W., Abu-Mahfouz, A. M., & Cheng, L. (2022). An optimization planning framework for allocating multiple distributed energy resources and electric vehicle charging stations in distribution networks. *Applied Energy*, *322*, 119513.
15. Zheng, W. Y., Wu, W. C., Zhang, B. M., Sun, H. B., & Liu, Y. B. (2016). A fully distributed reactive power optimization and control method for active distribution networks. *IEEE Transactions on Smart Grid*, *7*(2), 1021–1033.
16. Ma, W., Wang, W., Chen, Z., Wu, X. Z., Hu, R. N., Tang, F., & Zhang, W. G. (2021). Voltage regulation methods for active distribution networks considering the reactive power optimization of substations. *Applied Energy*, *284*, 116347.
17. Huang, Q., Tang, J., Li, H., & Nie, J. F. (2019). Reactive power optimization for distribution network based on improved bacterial chemotaxis particle swarm optimization. In *2019 12th international symposium on computational intelligence and design (ISCID)*, 14–15 Dec., Hangzhou, China. <https://doi.org/10.1109/ISCID.2019.00050>
18. Chen, G. G., Yi, X.-T., Zhang, Z.-Z., & Wang, H. M. (2018). Applications of multi-objective dimension-based firefly algorithm to optimize the power losses, emission, and cost in power systems. *Applied Soft Computing*, *68*, 322–342.
19. Bandopadhyay, J., & Roy, P. K. (2020). Application of hybrid multi-objective moth flame optimization technique for optimal performance of hybrid micro-grid system. *Applied Soft Computing*, *95*, 106487.
20. Arasteh, A., Alemi, P., & Beiraghi, M. (2021). Optimal allocation of photovoltaic/wind energy system in distribution network using meta-heuristic algorithm. *Applied Soft Computing*, *109*, 107594.
21. Ming, M. J., Trivedi, A., Wang, R., Srinivasan, D., & Zhang, T. (2021). A dual-population based evolutionary algorithm for constrained multi-objective optimization. *IEEE Transactions on Evolutionary Computation*, *25*(4), 739–753.
22. Jiang, T. X., Putrus, G., Gao, Z. W., Donald, S. M., & Wu, H. (2012). Analysis of the combined impact of small-scale wind generators and electric vehicles on future power networks. In *2012 47th international universities power engineering conference (UPEC)*, 4–7 Sept., Uxbridge, UK. <https://doi.org/10.1109/UPEC.2012.6398646>
23. Hetzer, J., Yu, D. C., & Bhattacharai, K. (2008). An economic dispatch model incorporating wind power. *IEEE Transactions on Energy Conversion*, *23*(2), 603–611.
24. Santos-Martin, D., Aranltes, S., & Amenedo, J. L. R. (2008). Reactive power capability of doubly fed asynchronous generators. *Electric Power Systems Research*, *78*(11), 1837–1840.
25. Brini, S., Abdallah, H. H., & Ouali, A. (2009). Economic dispatch for power system included wind and solar thermal energy. *The Leonardo Journal of Sciences*, *8*(14), 204–220.
26. Ma, Y. J., Liu, C., Zhou, X. S., & Gao, Z. Q. (2018). Reactive power compensation method for distribution network from electric vehicles. In *2018 37th Chinese control conference (CCC)*, 25–27 Jul., Wuhan, China <https://doi.org/10.23919/ChiCC.2018.8482930>
27. Wang, Y., Wang, T., Zhou, K. P., Cao, K., Cai, D. F., Liu, H. G., & Zhou, C. (2019). Reactive power optimization of wind farm considering reactive power regulation capacity of wind generators. In *2019 IEEE innovative smart grid technologies—Asia (ISGT Asia)*, 21–24 May, Chengdu, China. <https://doi.org/10.1109/ISGT-Asia.2019.8881439>
28. Lou, S. H., Wu, Y. W., Xiong, X. Y., & Tu, G. Y. (2006). A parallel PSO approach to multi-objective reactive power optimization with static voltage stability consideration. In *Transmission & distribution conference & exhibition*, 21–24 May, Dallas, USA. <https://doi.org/10.1109/TDC.2006.1668478>
29. Iba, K. (1994). Reactive power optimization by genetic algorithm. *IEEE Transactions on Power Systems*, *9*(2), 685–692.
30. Zhang, X. S., Tan, T., Yu, T., Yang, B., & Huang, X. M. (2020). Bi-objective optimization of real-time AGC dispatch in a performance-based frequency regulation market. *CSEE Journal of Power and Energy Systems*, 1–9.
31. Zhang, X. S., Li, C. Z., Xu, B., Pan, Z. N., & Yu, T. (2022). Dropout deep neural network assisted transfer learning for bi-objective Pareto AGC dispatch. *IEEE Transactions on Power Systems*.
32. Fan, Z., Li, W. J., Cai, X. Y., Li, H., Wei, C. M., Zhang, Q. F., Deb, K., & Goodman, E. (2020). Difficulty adjustable and scalable constrained multi-objective test problem toolkit. *Evolutionary Computation*, *28*(3), 339–378.
33. Fan, Z., Li, W. J., Cai, X. Y., Li, H., Wei, C. M., Zhang, Q. F., Deb, K., & Goodman, E. (2017). Push and pull search for solving constrained multi-objective optimization problems. *Swarm and Evolutionary Computation*, *44*, 665–679.
34. Fan, Z., Wang, Z. J., Li, W. J., Yuan, Y. T., You, Y. G., Yang, Z., Sun, F. Z., & Ruan, J. (2020). Push and pull search embedded in an M2M framework for solving constrained multiobjective optimization problems. *Swarm and Evolutionary Computation*, *54*, 100651.
35. Xu, B., Gong, D. W., Zhang, Y., Yang, S. X., Wang, L., Fan, Z., & Zhang, Y. G. (2022). Cooperative co-evolutionary algorithm for multi-objective optimization problems with changing decision variables. *Information Sciences*, *607*, 278–296.
36. Ma, Z. W., & Wang, Y. (2019). Evolutionary constrained multiobjective optimization: Test suite construction and performance comparisons. *IEEE Transactions on Evolutionary Computation*, *23*(6), 972–986.
37. Tian, Y., Zhang, T., Xiao, J. H., Zhang, X. Y., & Jin, Y. C. (2020). A coevolutionary framework for constrained multi-objective optimization problems. *IEEE Transactions on Evolutionary Computation*, *25*, 102–116.
38. Zille, H., Ishibuchi, H., Mostaghim, S., & Nojima, Y. (2017). A framework for large-scale multi-objective optimization based on problem transformation. *IEEE Transactions on Evolutionary Computation*, *22*(2), 260–275.